DOI: 10.1002/ejoc.201500740

D- and L-Mannose-Containing *glyco*-Oligoamides Show Distinct Recognition Properties When Interacting with DNA

M. Teresa Blázquez-Sánchez,[a,b] Filipa Marcelo,[c,d] María del Carmen Fernández-Alonso,[c] Rafael del Villar-Guerra,[a,e] Abdelouahid Samadi,[a] F. Javier Cañada,[c] Jesús Jiménez-Barbero,*[c,f,g] and Cristina Vicent*[a]

Keywords: Carbohydrates / Molecular recognition / Conformation analysis / NMR spectroscopy / DNA recognition

Mannose *glyco*-oligoamide β-D-Man-Py-γ-Py-Ind (β-D-Man, **1**) and two new *glyco*-oligoamides, β-L-Man-Py-γ-Py-Ind (β-L-Man, **2**) and 6-deoxy-β-D-Man-Py-γ-Py-Ind (6-deoxy-β-D-Man, **3**), have been designed and synthesized to investigate the role of hydrogen-bonding cooperative donor centres of carbohydrates in their recognition by DNA. The free- and bound-state geometries were studied, as were the affinities of the D and L enantiomers of the mannose *glyco*-oligoamides (**1** and **2**) for DNA polymers [ct-DNA and poly(dA-dT)$_2$]. TR-NOESY and DF-STD experiments for the diastereomeric complexes formed with DNA allow the asymmetric centres of the sugar residue that are close to the inner and outer regions of the DNA minor grooves to be distinguished. A C→N hairpin folding in β-L-Man derivative **2** was observed, with the α face of the sugar close to the indole ring. The C-2 and C-3 centres are orientated towards the inner region of the DNA minor groove. The affinity data for poly(dA-dT)$_2$ indicate that there is a chiral discrimination process, with β-L-Man derivative **2** being the best ligand. 6-Deoxy-β-D-Man derivative **3** forms the least stable complexes with DNA. Molecular dynamics simulations of β-L-Man derivative **2** in complex with a double-strand dodecamer d(AT)$_{12}$ are in agreement with the experimental NMR spectroscopic data. Thus, the cooperative donor centre 2-OH in the L-mannose enantiomer is a key contributor to the stability of the **2**·poly(dA-dT)$_2$ complex.

Introduction

It is vitally important to understand the fine structural details involved in molecular recognition processes if the related chemical and/or biological events are to be modulated and influenced.[1] In this context, sugar recognition by receptors is now a key research area, given its involvement in multiple events relevant to biomedicine. Hydrogen bonds and CH–π interactions form the basis of the recognition of neutral carbohydrates by lectins.[2] In contrast, for the binding of carbohydrates to the minor groove of DNA, the relative importance of the forces that form the basis of the complexation event are not precisely known.[3] The ability of carbohydrates to form hydrogen bonds with the base-pair donor and acceptor centres and the phosphate group should be considered. Indeed, one way to increase the affinity and the directionality of these forces would be to make use of hydrogen-bonding cooperativity[4] (see Figure 1).

Hydrogen-bond cooperativity has been evaluated in non-polar solvents,[5] but the effect of intramolecular hydrogen bonds on intermolecular hydrogen bonds in water has never been evaluated.[6] As illustrated in Figure 1, we have previously reported on the survival of an intramolecular NH···2-OH bond in water for the *glyco*-oligoamide β-D-Man-Py-γ-Py-Ind (**1**).[7] This directional intramolecular hydrogen bond might allow 2-OH to behave as a cooperative donor in an intermolecular process. In the work presented in this paper, we have explored the use of hydrogen-bonding cooperativity for carbohydrate–DNA recognition. Thus, we describe the synthesis, conformational analysis, and binding properties of three mannose derivatives: β-D-Man (**1**), β-L-Man (**2**), and 6-deoxy-β-D-Man (**3**) (Figure 1). These chemical entities allow the presence of one directional intramolecular hydrogen bond between the 1-NH amide at the anomeric position and 2-OH (see Figure 1), which adopts an axial orientation in the mannose six-membered ring. We planned to use both D- and L-mannose

[a] SEPCO Department, Instituto de Química Orgánica General, IQOG-CSIC,
Juan de la Cierva 3, 28006 Madrid, Spain
E-mail: cvicent@iqog.csic.es
http://www.iqog.csic.es/iqog/es/CristinaVicent/homepage
[b] Current address: School of Chemistry and Chemical Biology, University College Dublin,
Belfield, Dublin 4, Ireland
[c] Centro de Investigaciones Biológicas, CIB-CSIC,
Ramiro de Maezty 9, 28049 Madrid, Spain
[d] Current address: UCIBIO, REQUIMTE, Faculdade Ciencias e Tecnologia, Universidade Nova de Lisboa,
2829-516, Caparica, Portugal
[e] Current address: James Graham Brown Cancer Center, University of Louisville, Clinical and Translation Research,
505 S. Hancock Street, Louisville, KY 40202, USA
[f] Infectious Disease Programme, CICbioGUNE,
48160 Derio, Bizkaia, Spain
[g] IKERBASKE, Basque Foundation for Science,
48011 Bilbao, Spain
Supporting information for this article is available on the WWW under http://dx.doi.org/10.1002/ejoc.201500740.

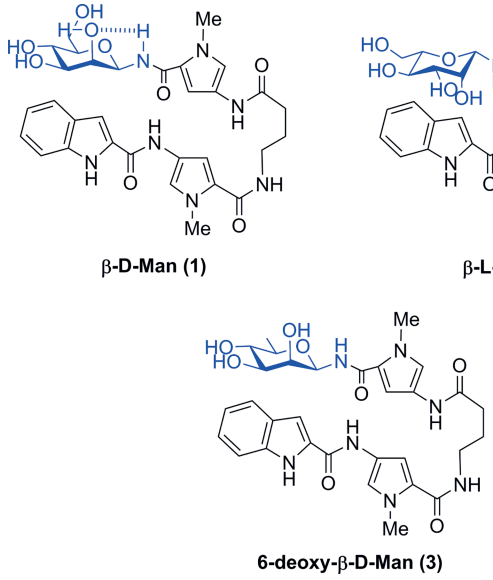

Figure 1. Structure of *glyco*-oligoamides **1**–**3**.

enantiomers (**1** and **2**) so as to provide diastereomeric complexes that would allow the asymmetric centres of the respective sugars to reach the complementary strand of the minor groove of the B-DNA in different ways, always depending on the folding adopted by the *glyco*-oligoamide. Indeed, previous works by Chaires[8] and Dervan[9] have described the benefit of using both enantiomers of a DNA minor-groove chiral ligand for binding to the target DNA sequence. This approach should provide relevant and distinct effects regarding the binding at the minor groove. We also planned to assess the role of 6-OH in the recognition process (Figure 1) by studying 6-deoxy derivative **3**.

Results and Discussion

Synthesis and Structural Studies of *glyco*-Oligoamides 1–3

A retrosynthetic analysis of *glyco*-oligoamides **1**–**3** is shown in Scheme 1. This route has previously been used[10] to obtain neutral *glyco*-oligoamides with different substitution at pyrrole B, close to the sugar moiety, The key coupling reaction between glycosylamine **II** and activated carboxylic acid **III** at the C terminal of the oligoamide was performed in the solution phase to give the β-*glyco*-oligoamides in good yields (see below).

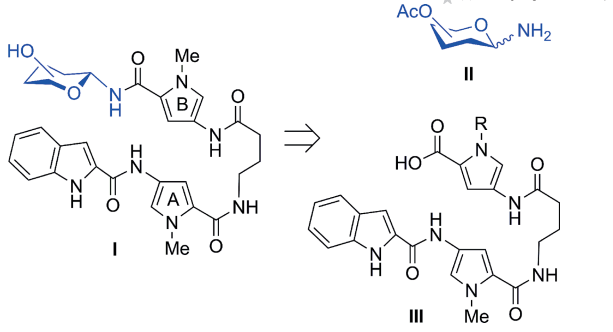

Scheme 1. Retrosynthetic strategy for the synthesis of sugar-oligoamide **I**.

The synthesis of glycosylamine precursors **8** and **9** (**II** in Scheme 1) was carried out following the synthetic sequence shown in Scheme 2. Compounds **4** and **5** were obtained by acetylation of the free sugars using either Ac_2O/py or NaOAc/Ac_2O in good yields (80–86%). The corresponding azides were synthesized by treatment with $SnCl_4$ and trimethylsilyl azide[11] in 70–90% yields. Finally, catalytic hydrogenation (5% Pd/C, MeOH)[12] of the azide generated the corresponding D and L amino sugars (Scheme 2), which were used in the next step without further purification.

The synthesis of 6-deoxy-amine derivative **15** involved a different route (Scheme 3). The key step was the removal of the hydroxy group at C-6. The primary alcohol of D-mannose was tosylated, and then the addition of acetic anhydride[13] gave **10** as a mixture of pyranose anomers in 97% yield. Removal of the tosyl group by C-6 iodination with potassium iodide gave compound **11** in 61% yield. Raney Ni reduction produced the desired compound (i.e., **13**) in 23% yield, together with derivative **12**, deprotected at the anomeric position, in 60% yield (see Exp. Sect. and Figure S8 in the Supporting Information). Compound **12** was acetylated with pyridine and anhydride acetic to give more compound **13** (95% yield). Azidation of **13** with trimethylsilyl azide and $SnCl_4$ gave[11] **14**, and then hydrogenation (5% Pd/C, MeOH) gave amine **15** in 95% yield.

After obtaining the three protected glycosylamines **8**, **9**, and **15**, the next step in the synthesis was the formation of the β-configured amidoglycosidic bonds. The addition–elimination reaction between the glycosylamines and activated carboxylic acid **16**[10] in DMF/DIEA (diisopropylethylamine) gave the corresponding acetylated *glyco*-oligoamides (i.e., **17**–**19**) in yields of 28–70%. (Scheme 4).

The common last step in the synthesis of the new *glyco*-oligoamides (Figure 1) was the deprotection of acetylated

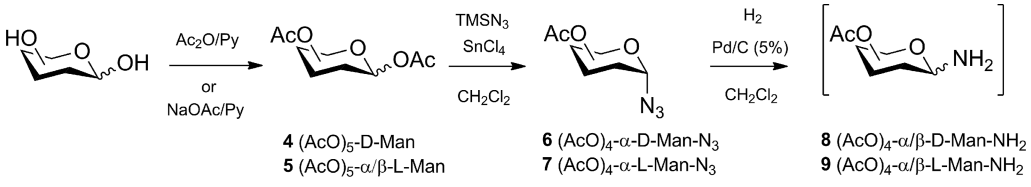

Scheme 2. Synthesis of glycosylamines **8** and **9**.

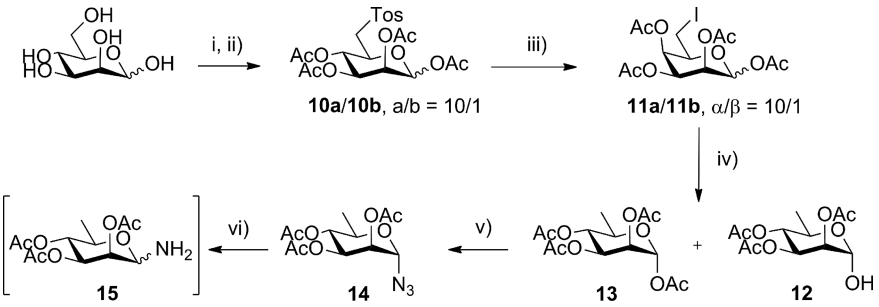

Scheme 3. Synthesis of β-glycosylamine **15**. i) TsCl, py; ii) Ac_2O; iii) KI, 100 °C; iv) Raney Ni, py; v) $TMSN_3$ (trimethylsilyl azide), $SnCl_4$; vi) H_2, 5% Pd/C, MeOH.

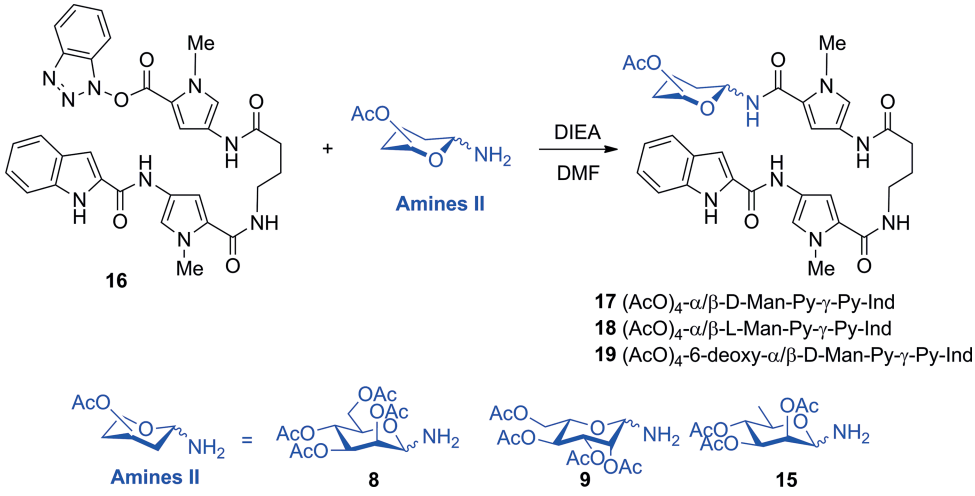

Scheme 4. General scheme for the synthesis of protected sugar-oligoamides **17**–**19**.

compounds **17**–**19**. This was achieved using MeONa/MeOH[10,14] to give the target water soluble β-sugar-oligoamides (i.e., **1**–**3**) in yields of 70–79%.

Before studying the structural data of **1**–**3** in the DNA-bound state, the conformation of the ligands in the free state was assessed by NMR spectroscopy at 5 and 25 °C. We have previously characterized a hairpin structure for free *glyco*-oligoamides with equatorial 2-OH groups.[10,15] Following an analogous protocol, compound **1** (β-D-Man) was shown to have a hairpin-like conformation, with its α face pointing towards the indole ring.[7] The NMR spectroscopic data for **2** and **3** in the free state (Figure S18 in the Supporting Information) also indicated the presence of a major hairpin structure. This conclusion was based on the nOes observed at 5 °C, especially those between the protons of both of the pyrrole units and those between the carbohydrate and the indole residues (in red in Figure S18 in the Supporting Information). Additionally, intra-strand nOes between the NH's and the aromatic signals of the pyrroles and indole at 5 °C in H_2O (in green in Figure S18 in the Supporting Information) also provided unambiguous information on the existence of a crescent hairpin structure with two well-defined different rims (the N-Me rim and NH rim).

These nOes show that the sugar residue of each of the D- and L-mannose *glyco*-oligoamides (i.e., **1**–**3**) presents its α face pointing towards the indole ring, while the C-2 and C-3 centres are orientated towards the NH rim (Figure 2). The combined information of nOes and $J_{NH\text{-}5,1\text{-}H}$ coupling constants (ca. 9.0 Hz in all three cases) is compatible only with an N→C folding (Structure A in Figure 2) in the free state for **1** and **3** (D-Man), while **2** (L-Man) shows a C→N folding (Structure B in Figure 2).

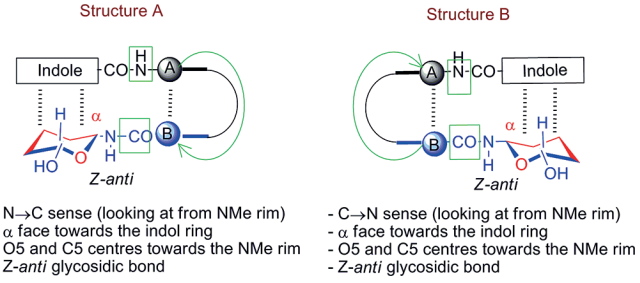

Figure 2. Schematic view of the different folding possibilities of **1**–**3**.

According to the hairpin-like conformation, the NH and CH_3 rims can be defined as schematically presented in Figure 3.

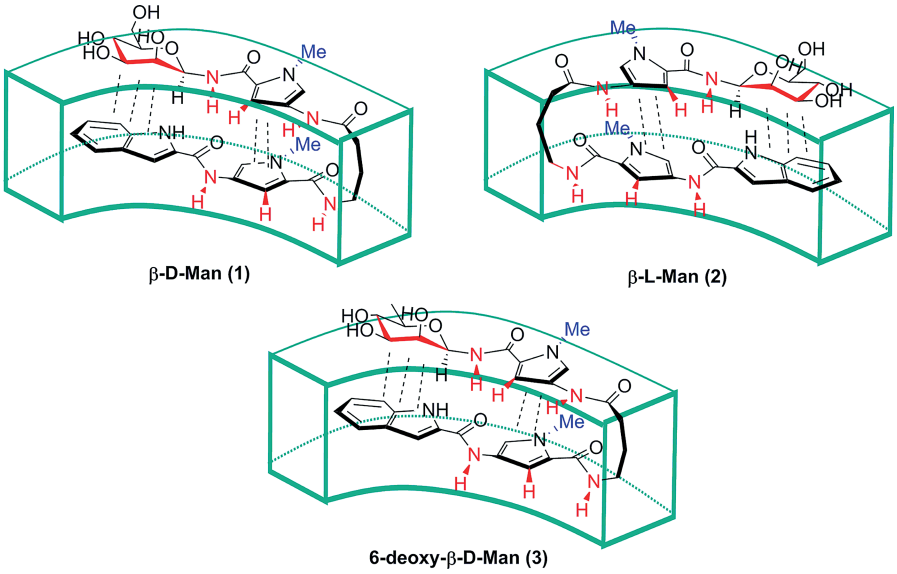

Figure 3. Schematic structure of the *glyco*-oligoamides with the definition of the two rims and the two possible folding modes.

Inspection of the obtained geometries indicated that, for these molecules, the cooperative centre 2-OH is orientated towards the NH rim. Thus, if the conformation in the free state is retained in the bound state, the cooperative centre in the sugar should be orientated towards the inner region of the DNA minor groove.

Interaction Studies with DNA Polymers [ct-DNA and Poly(dA-dT)$_2$]

Two DNA polymers were used for the DNA-binding studies. These two polymers, ct-DNA and poly(dA-dT)$_2$, were chosen as models of random and defined DNA sequences, respectively, to assess the preferred DNA-binding sequence of the three ligands using NMR experiments. The structural features of the complexes of **1**–**3** were evaluated by TR-NOESY and differential-frequency saturation-transfer difference[16] (DF-STD) experiments. In this manner, information about the conformation of the ligands and the orientation of the asymmetric centres of the carbohydrate in the DNA minor groove were deduced. Moreover, estimation of the binding affinities of **1**–**3** by ^{1}H NMR titration and competition experiments provided a relationship between the structural and affinity data. First, the DNA-sequence preference of *glyco*-oligoamides **1**–**3** was checked by titration experiments with ct-DNA and poly(dA-dT)$_2$ in a qualitative manner. In particular, increasing amounts of the polymer were added to a constant-concentration solution of *glyco*-oligoamide **1**. For both ct-DNA and poly(dA-dT)$_2$, a significant line-broadening of the resonances of **1** was always observed (Figure S19 in the Supporting Information). However, the intensities of the aromatic signals of the ligand were observed to decrease earlier for the additions to poly(dA-dT)$_2$, which strongly suggests that binding to this DNA polymer is preferred (Figsures S19 and S20 in the Supporting Information).

The conformation of the *glyco*-oligoamides in the bound state was deduced from TR-NOESY experiments with both DNA polymers. Negative and intense nOes were always observed, consistent with the nOes detected in the free state (Figure 4). A clear hairpin conformation was characterized in the bound state thanks to the presence of inter-strand contacts between pyrrole A and pyrrole B resonances (common nOes: P5A–MeB and P5B–MeA) in both complexes for all three ligands **1**–**3**. (For nomenclature and numbering of the *glyco*-oligoamides, see the Supporting Information, Figure 4 and also Figures S21–S27 in the Supporting Information). Additional carbohydrate–indole nOes were also found for the complexes of β-L-Man (**2**) bound to both ct-DNA (1-H–Ind-3, 2-H–Ind-3, 2-H–Ind-4, 3-H–Ind-4, 3-H–Ind-5) and poly(dA-dT)$_2$ (1-H–Ind-3). Thus, these findings reveal that the hairpin structure is better defined in these two complexes with **2**. Moreover, these experimental results show the proximity of the α face of the L-mannose sugar to the indole ring in the DNA-bound state, irrespective of the DNA source.

Additional information on the geometry (folding directionality) of the complexes was deduced from DF-STD experiments. These experiments have been used as a tool to distinguish between the three principal ligand–DNA binding modes.[16] The difference between the horizontal and vertical dimensions of DNA generate an anisotropic effect causing a saturation diffusion with a different efficacy along the axis of the macromolecule. In this manner, information about the proximity of the different regions of **1**–**3** to the internal and external regions of the minor groove in the two different DNA complexes was obtained.

Two parallel sets of STD experiments were performed for every complex of **1**–**3** with ct-DNA[17] and poly(dA-dT)$_2$. In one of them, the 4′-H/5′-H/5′′-H spectral region (outer region of the minor groove, I_{out}) was saturated. In the alternative experiment, the 1′-H (inner region, I_{in}) resonance

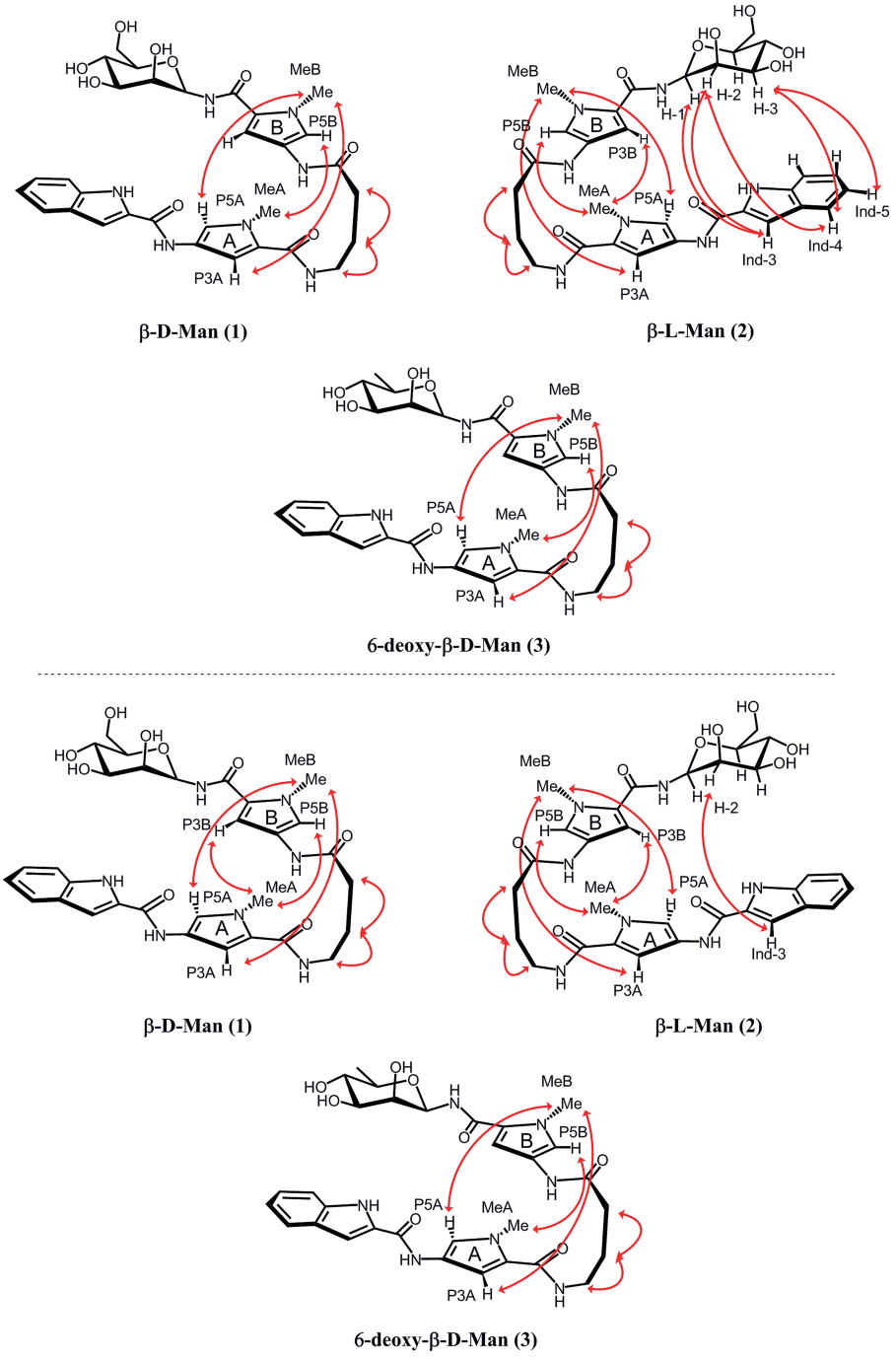

Figure 4. Schematic representation of the conclusions extracted from the analysis of the TR-NOESY experiments. Above: Interstrand nOes of **1**–**3** in the bound state to ct-DNA. Below: Interstrand nOes of **1**–**3** in the bound state to poly(dA-dT)$_2$.

was chosen for saturation. Figure S28 in the Supporting Information shows an example of the resulting ^{1}H-STD experiment for the two different selected irradiation frequencies in the outer and in the inner regions of the minor groove. Figure S29 in the Supporting Information gathers a summary of the STD results of the bound states of **1**–**3** to both ct-DNA and poly(dA-dT)$_2$. It is important to highlight that the magnetization is transferred to the whole molecule, including the sugar residue, which indicates that all parts of each of the ligands are inside the minor groove in all of the DNA complexes. Furthermore, the distribution of the saturation is similar within the oligoamide parts of **1**–**3** in each of the ct-DNA and poly(dA-dT)$_2$ complexes, which strongly suggests a similar binding mode for this part of the ligand in all cases. (Figure S29 in the Supporting Information). In contrast, for the proton resonances of the carbohydrate moiety, the STD intensity ratio values (I_{out}/I_{in}) were rather different (Figure S30 in the Supporting In-

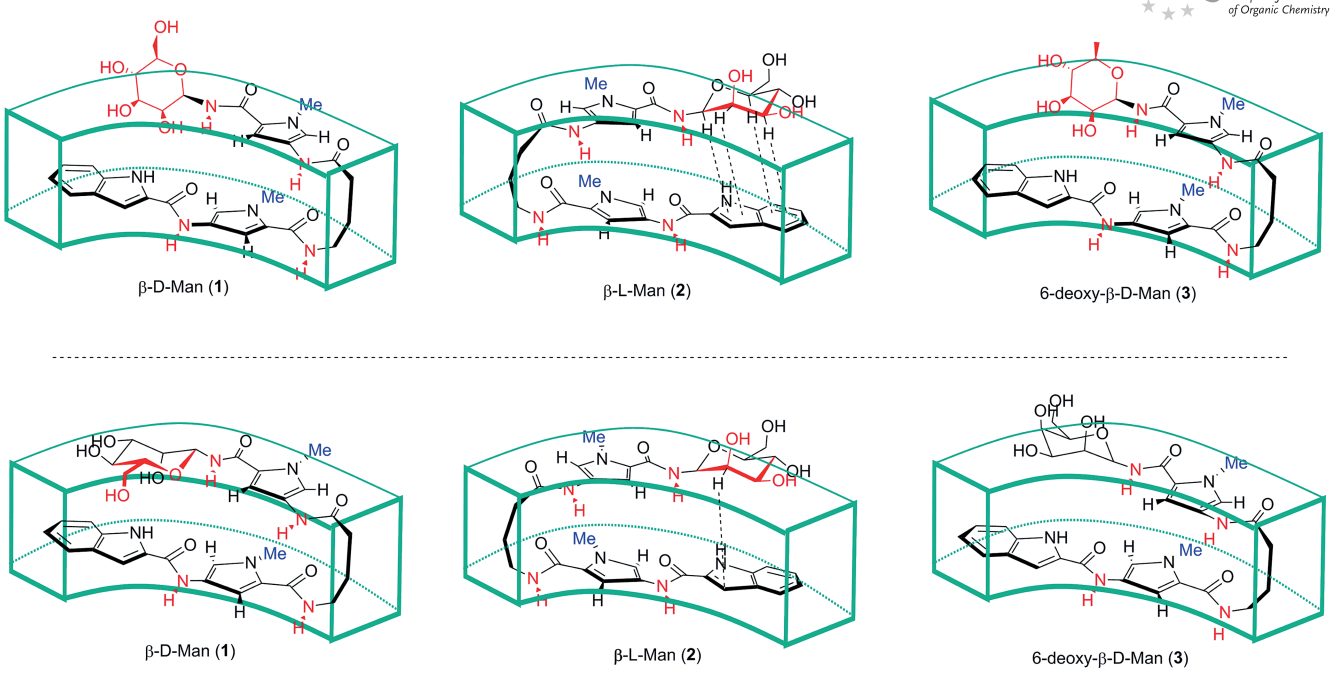

Figure 5. Schematic view of the presentation mode of *glyco*-oligoamides **1**–**3** with ct-DNA (above) and poly(dA-dT)$_2$ (below) as deduced from TR-NOESY and STD experiments for the complexes.

formation) for the different complexes. The smallest values corresponded to the atoms closer to the inner region of the minor groove, while the biggest ones corresponded to those closer to the outer region of the minor groove. Consequently, for the ct-DNA complex, D-Man derivatives **1** and **3** place the β face of the sugar towards the inner region of the minor groove. On the other hand, there is a different orientation in the complex with poly(dA-dT)$_2$. In this case, for β-D-Man derivative **1**, the C-5 and C-6 centres are those pointing towards the inner region of the minor groove; no well-defined presentation could be found for **3**. Fittingly, for β-L-Man derivative **2**, the mannose C-2 and C-3 centres are always orientated towards the inner region of the minor groove. Thus, in this case, the predicted cooperative hydrogen-bond donor centre 2-OH is in the minor groove of both ct-DNA and poly(dA-dT)$_2$, where it could be involved in interactions with hydrogen-bond acceptor centres.

Thus, the combined information from TR-NOESY and STD NMR spectroscopic data allow us to postulate a presentation mode for these molecules towards the DNA molecules, as illustrated in Figure 5.

In fact, only for the complexes of **2**, did the experimental NMR spectroscopic data allow us to determine the folding direction in an unambiguous manner. For both of the complexes of **2**, we found carbohydrate-to-indole nOes that demonstrate that the indole moiety is in close contact with the α face of the mannose ring. Furthermore, the STD data demonstrate that the C-2 and C-3 centres of the L-mannose are presented to the inner region of the minor groove. This combined information can only be accounted for by a C→N folding of β-L-Man derivative **2** in the minor groove. (Figure 6).

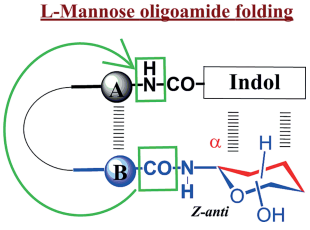

Figure 6. Schematic representation of the C→N folding of the *glyco*-oligoamide **2** in the complex with ct-DNA and poly-(dA-dT)$_2$.

Therefore, the bound geometry of **2** highly resembles that which it has in the free state, suggesting a high degree of preorganization of this ligand. This fact allows us to postulate that there is a minor entropy penalty for the binding process. Thus, the presentation of 2-OH towards the inner region of the minor groove is consistent with the higher binding affinity of this ligand compared with its enantiomer.

Binding Affinities. Relative K_d Values of the Ligands 1–3 with Poly(dA-dT)$_2$ Measured by ^{1}H NMR Spectroscopy

The binding affinities were estimated by using ^{1}H NMR titration experiments, as described in the Exp. Section. The three molecules behaved differently. Indeed, significant differences were found in the amount of poly(dA-dT)$_2$ needed to produce a similar effect on the ligand signals (Figures S32–S34 in the Supporting Information). Table 1 shows the obtained K_d values together with the concentra-

tions of the ligands, and the *c* values (see Exp. Sect. for definition).

Table 1. K_d values obtained by data fitting for different proton resonances Ind-3, P3A, P5A, P3B, P5B, MeA, and MeB of *glyco*-oligoamides **1**–**3** in their interaction with poly(dA-dT)$_2$.

Proton[a]	*c*	β-D-Man	β-L-Man	6-deoxy-β-D-Man (**3**)
Ind-3	40	3.2	1.2	6.6
P5A	25	2.7	1.3	7.0
P3A	22	2.5	1.3	11.2
P5B	13	1.3[c]	0.2[c]	3.2
P3B	10	3.2	0.9	4.1
MeA	55	2.9	0.7	5.7
MeB	30	3.0	0.3	7.2
K_d [mM] [a][b]		2.9 ± 0.4	0.9 ± 0.4	6.1 ± 1.3
[ligand] [μM]		250	100	170

[a] The concentrations of the dissociation constants are expressed in mM base pair (bp). [b] The dissociation constants are the arithmetical average of the values measured for the different resonances. The errors were calculated as the standard deviation of the average K_d. [c] Excluded values from averaging.

The K_d values indicate that β-L-Man *glyco*-oligoamide **2** is the best binder, while 6-deoxy-β-D-Man derivative **3** is the worst. The comparison between **1** and **3** shows that 6-OH plays a significant role in the complexation. This fact is in agreement with the NMR spectroscopic data obtained for **1**, which indicated that 6-OH was orientated towards the inner region of the minor groove in poly(dA-dT)$_2$ binding.

The titration experiments were further validated by performing competition experiments between pairs of ligands in the presence of poly(dA-dT)$_2$, as described in the Exp. Section. The results for the competition of **1** vs. **3** with poly(dA-dT)$_2$ are gathered in Figure 7. Upon addition of the DNA, the resonances of **1** broadened significantly, and their intensities diminished much faster than those of **3**. This evidence supports the conclusions of the titration experiments, which also showed that **1** interacts with poly-(dA-dT)$_2$ much more strongly than **3**.

Calculations

Finally, a 3D structure of the most stable complex was derived using MD (molecular dynamics) simulations. A hairpin conformation of **2** was chosen as starting geometry for the ligand (as deduced by the NMR spectroscopic analysis), A double-strand dodecamer d(AT)$_{12}$ sequence was chosen as a model for the DNA. The MD simulations showed that a stable complex is formed. Indeed, the minimized starting geometry of the complex was fairly stable, in agreement with the NMR-based experimental conclusions. Ligand **2** adopts a hairpin conformation with a C→N folding. Interestingly, π–π and CH–π intramolecular interactions are present within the ligand. The ligand is inserted into the minor groove of the oligomer. Regarding the carbohydrate moiety, it is important to mention that the α face of the L-mannose moiety is pointing towards the indole ring, and the C-2 and C-3 centres of the sugar are orientated towards the inner region of the groove, inside the minor groove, as expected from the NMR spectroscopy results. Figure 8 shows some details of the interactions, including the intramolecular hydrogen bond between 5-NH and 2-OH of β-L-Man derivative **2**. Additionally, hydrogen bond interactions from the bases to 2-OH of the L-mannose residue could also be observed. Indeed, the simulation shows two intermolecular hydrogen bonds between this particular residue of the ligand and the base pairs in the minor groove. This detail supports the presence of a cooperative intermolecular hydrogen bond in this complex. Fittingly, there are remarkable structural differences with the complex of β-D-Man derivative **1** with poly-(dA-dT)$_2$. In this case, C-2 of the sugar was pointing to the outer region of the groove, with a completely different presentation.

These structural differences may account for the different binding abilities found for the two enantiomers with poly-(dA-dT)$_2$.

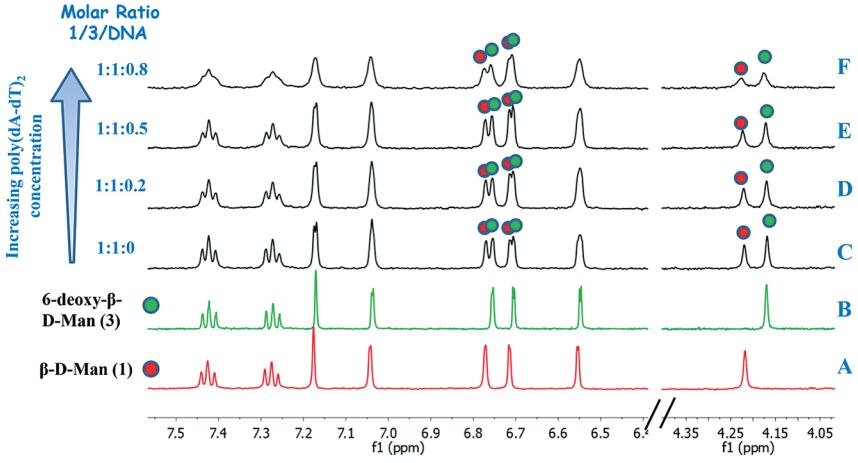

Figure 7. Competition experiment between **1** and **3** with poly(dA-dT)$_2$. A) Expanded aromatic region of the signals of the ^{1}H NMR spectrum of **1** in the absence of poly(dA-dT)$_2$ in red. B) Expanded aromatic region of the signals of the ^{1}H NMR spectrum of **3** in the absence of poly(dA-dT)$_2$ in green. C) Spectrum of a mixture of **1** and **3** (*c* = 155 μM for both compounds) in the absence of DNA. D–F) Spectra of a mixture of **1** and **3** in the presence of increasing amounts of poly(dA-dT)$_2$: D) 31 μM (base pair = bp), E) 77 μM (bp), F) 124 μM (bp). All spectra were recorded with 64 scans with a 500 MHz spectrometer using phosphate buffer at 25 °C.

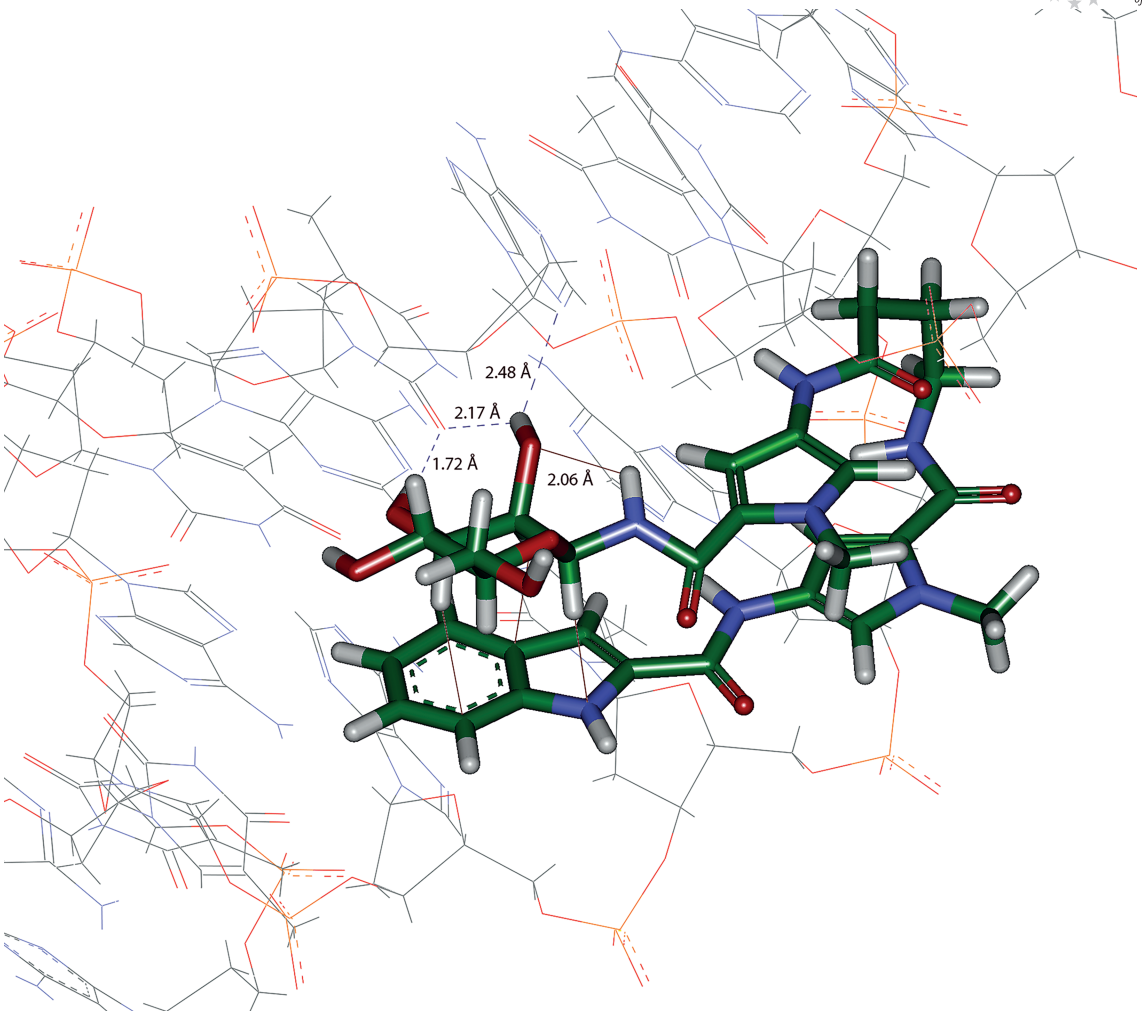

Figure 8. Structure of β-L-Man (**2**)/double-strand dodecamer $d(AT)_{12}$ complex during the MD simulations in explicit water.

Conclusions

Three mannose *glyco*-oligoamide ligands (**1**, **2**, and **3**) have been synthesized as model compounds to investigate the fine structural details of sugar–DNA interactions. Their water solution conformations indicate that they have a hairpin conformation, although the folding adopted by the hairpin is rather different, depending on the sugar stereochemistry. In both enantiomers **1** and **2**, the α face of the mannose unit is close to the indole, while C-2 and C-3 are close to the NH rim. This orientation permits the putative cooperative centre 2-OH to be orientated towards the NH rim, ready to interact with the inner region of an encountering DNA groove.[3]

All three derivatives are ligands for ct-DNA and poly-$(dA\text{-}dT)_2$. Qualitatively, the ^1H NMR titration experiment suggests a certain selectivity for ATAT. The bound conformation of the ligands in the presence of ct-DNA and poly$(dA\text{-}dT)_2$ was determined using TR-NOESY and STD experiments. The β-L-Man analogue (**2**) shows a hairpin conformation with an N→C folding direction in the bound state, with the α face of the L-mannose residue orientated towards the indole ring. This orientation resembles that which is also found in the free state.

The sugar orientation is ill-defined in the complexes of **1** and **3**. The STD data also allowed an assessment of the relative orientation of the ligand in the DNA minor groove, especially for **1** and **2**. In particular, **1** orientated its C-2 centre towards the outer region of the minor groove when bound to poly$(dA\text{-}dT)_2$, while the C-2 centre of β-L-Man (**2**) pointed towards the inner region of the minor groove in both DNA complexes. This latter inward-pointing orientation allows the corresponding 2-OH to be involved in an intermolecular hydrogen bond with the acceptor moieties in the DNA groove.

Indeed, the binding experiments have shown that L enantiomer **2** shows better binding to poly$(dA\text{-}dT)_2$ than do the two D analogues. The role of 6-OH in the interaction process has also been investigated. The binding affinity of **1** is two times greater than that of **3**. In fact, **3** did not show a clear orientation of the sugar centres in the bound states.

The use of molecular dynamics simulations of the complex of **2** with a double-strand dodecamer $d(AT)_{12}$ gave a 3D perspective of the interaction. The calculations suggest that there are two intermolecular hydrogen bonds involving 2-OH of L-Man and the acceptor centres in the minor groove of DNA, as well as a variety of intramolecular interactions; they indicate the presence of an intramolecular 5-NH–2-OH hydrogen bond.

These results suggest that there is a correlation between the association constant values and the presentation of the ligand relative to the DNA, with a special role for the C-2 centre in the L-Man *glyco*-oligoamide. This demonstrates the importance of cooperative hydrogen bonding in providing effective intermolecular sugar–DNA interactions in the minor groove.

Experimental Section

General Procedures: All reactions with sensitive reactants were carried out under an argon atmosphere. Solvents and reactants were purchased from Sigma–Aldrich, Fluka, Merck, and Acros, and were purified when necessary. A purification system PS-400-3-MD for drying solvents was used to remove residual water. The H_2O used for NMR studies was freshly filtered milli-Q water. Flash chromatography was carried out with silica gel 60 (230–400 ASTM mesh). Silica gel 60 F254 aluminum-backed TLC plates of 0.2 mm thickness were used to monitor the reactions. NMR spectra were obtained with Varian Innova 300 (300 MHz), Varian Innova 400 (400 MHz), and Bruker Avance 500 MHz spectrometers. COSY, HSQC, and HMBC 2D NMR experiments were performed for further assignment of the structures when required. Chemical shifts were referenced using residual solvent peaks: $CDCl_3$, δ = 7.26 ppm for ^{1}H NMR, and 77.00 ppm for ^{13}C NMR; [D_6]DMSO, δ = 2.50 ppm for ^{1}H NMR, and 39.43 ppm for ^{13}C NMR; [D_4]methanol, δ = 3.31 ppm for ^{1}H NMR, and 49.00 ppm for ^{13}C NMR; and [D_6]acetone, δ = 2.06 ppm for ^{1}H NMR, and 30.84/206.7 ppm for ^{13}C NMR. Optical rotations were measured with a Perkin–Elmer 241MC polarimeter at room temperature in a 1.0 dm cell. Mass spectrometry was carried out with an HP series 1100 MSD instrument. Elemental analyses were measured with a Carla Erba CHNS-O EA1108 elemental analyser.

Compounds **4**,[18] **6**,[19] **8**,[11,19] **10**,[20] **11**,[20,21] **13**,[22] and **14**[5a] have been described previously in the literature.

1,2,3,4,6-Penta-*O*-acetyl-α/β-L-mannopyranose (5): A mixture of L-mannose (1.0 g, 5.55 mmol), acetic anhydride (10.0 mL), and pyridine (15 mL) was stirred at room temperature for 10 h. Toluene was added, and then the solvents were removed under reduced pressure. The crude material was purified by column chromatography (hexane/ethyl acetate, 1:1) to give compound **5** (1.87 g, 86%) as a mixture of α/β pyranose anomers (1:0.16). An analytical sample of the α pyranose anomer was isolated for complete characterization. Data for the α anomer: R_f = 0.27 (diethyl ether/pentane, 3:2). $[\alpha]_D$ = –54.3 (c = 2.6 in $CHCl_3$). ^{1}H NMR (500 MHz, $CDCl_3$): δ = 2.00 (s, 3 H, CH_3, AcO), 2.04 (s, 3 H, CH_3, AcO), 2.08 (s, 3 H, CH_3, AcO), 2.16 (s, 3 H, CH_3, AcO), 2.17 (s, 3 H, CH_3, AcO), 4.02–4.06 (m, 1 H, 5-H), 4.00 (dd, J = 12.4, 2.5 Hz, 1 H, 6-H), 4.27 (dd, J = 12.4, 4.9 Hz, 1 H, 6′-H), 5.25 (t, J = 2.2 Hz, 1 H, 2-H), 5.33–5.35 (m, 2 H, 3-H, 4-H), 6.08 (d, J = 1.9 Hz, 1 H, 1-H) ppm. ^{13}C NMR (125 MHz, $CDCl_3$): δ = 20.76 (CH_3, AcO), 20.78 (CH_3, AcO), 20.84 (CH_3, AcO), 20.89 (CH_3, AcO), 20.99 (CH_3, AcO), 62.2 (CH_2, C-6), 65.6 (CH, C-4), 68.4 (CH, C-2), 68.8 (CH, C-3), 70.7 (CH, C-5), 90.7 (CH, C-1), 168.2 (CO, AcO), 169.6 (CO, AcO), 169.8 (CO, AcO), 170.1 (CO, AcO), 170.7 (CO, AcO) ppm. HRMS (ESI$^+$): calcd. for $C_{16}H_{26}NO_{11}$ [M + NH_4]$^+$ 408.1500; found 408.1499. IR (film): $\tilde{\nu}$ = 2962, 1752, 1370, 1220, 1149, 1088, 1053, 1026, 974, 755 cm^{-1}. $C_{16}H_{22}O_{11}$ (390.34): calcd. C 49.23, H 5.68; found C 49.51, H 5.84.

2,3,4,6-Tetra-*O*-acetyl-α-L-mannopyranosyl Azide (7): Compound **7** was prepared from **5** (1.6 g, 4.1 mmol) analogously to the synthesis of **6**.[19] The crude material was purified by column chromatography to give compound **7** (1.10 g, 70%). R_f = 0.23 (diethyl ether/pentane, 2:3). $[\alpha]_D$ = –120.9 (c = 3.9, $CHCl_3$). ^{1}H NMR (500 MHz, $CDCl_3$): δ = 1.99 (s, 3 H, AcO), 2.05 (s, 3 H, AcO), 2.11 (s, 3 H, AcO), 2.16 (s, 3 H, AcO), 4.12–4.17 (m, 1 H, 5-H), 4.18 (d, J = 2.4 Hz, 6-H), 4.30 (dd, J = 12.5, 5.6 Hz, 1 H, 6′-H), 5.15 (dd, J = 3.1, 1.9 Hz, 1 H, 2-H), 5.23–5.31 (m, 2 H, 3-H, 4-H), 5.38 (d, J = 1.9 Hz, 1 H, 1-H) ppm. ^{13}C NMR (125 MHz, $CDCl_3$): δ = 20.75 (CH_3, AcO), 20.81 (CH_3, AcO), 20.85 (CH_3, AcO), 20.96 (CH_3, AcO), 62.28 (CH_2, C-6), 65.76 (CH, C-4), 68.37 (CH, C-3), 69.32 (CH, C-2), 70.77 (CH, C-5), 87.60 (CH, C-1), 169.76 (CO, AcO), 169.87 (CO, AcO), 169.99 (CO, AcO), 170.72 (CO, AcO) ppm. HRMS (ESI$^+$): calcd. for $C_{14}H_{23}N_4O_9$ [M + NH_4]$^+$ 391.1460; found 391.1457. IR (film): $\tilde{\nu}$ = 3637, 3438, 3390, 2960, 2464, 2122, 1748, 1434, 1371, 1223, 1125, 1085, 1053, 960 cm^{-1}. $C_{14}H_{29}N_3O_9$ (383.40): calcd. C 45.04, H 5.13, N 11.26; found C 45.14, H 5.30, N 11.17.

2,3,4,6-Tetra-*O*-acetyl-α/β-L-mannopyranosylamine (9): Pd/C (5%; 0.25 g) was added to a solution of **7** (0.5 g, 1.34 mmol) in anhydrous CH_2Cl_2. The mixture was stirred under H_2 at atmospheric pressure for 2 h. The Pd/C was removed by filtration through a nylon filter. The filtrate was concentrated in vacuo to remove the CH_2Cl_2 and give compound **9** (0.44 g, 95%) as a mixture of α/β anomers (0.15:1), which was used without further purification. The mixture of α and β anomers is described as follows: R_f = 0.13 (hexane/EtOAc, 2:1). ^{1}H NMR (500 MHz, $CDCl_3$): δ = 1.98 (s, 3 H, AcO, β anomer), 2.02 (s, 3 H, AcO, α anomer), 2.04 (s, 3 H, AcO, β anomer), 2.06 (s, 3 H, AcO, α anomer), 2.10 (s, 6 H, 2 AcO, α and β anomers), 2.15 (s, 3 H, AcO, α anomer), 2.20 (s, 3 H, AcO, β anomer), 3.67 (ddd, J = 9.9, 5.6, 2.4 Hz, 1 H, 5-H, β anomer), 4.02–4.06 (m, 1 H, 6-H, α anomer), 4.11 (dd, J = 12.2, 2.3 Hz, 1 H, 6-H, β anomer), 4.25 (dd, J = 12.2, 5.6 Hz, 1 H, 6′-H, β anomer), 4.29–4.35 (m, 2 H, 5-H, 6′-H, α anomer), 4.47 (s, 1 H, 1-H, β anomer), 4.90 (d, J = 2.5 Hz, 1 H, 1-H, α anomer), 5.07 (dd, J = 10.1, 3.4 Hz, 1 H, 3-H, β anomer), 5.19 (t, J = 10.0 Hz, 1 H, 4-H, β anomer), 5.21–5.26 (m, 2 H, 2-H, 4-H, α anomer), 5.34 (dd, J = 9.2, 3.4 Hz, 1 H, 3-H, α anomer), 5.41 (dd, J = 3.4, 1.1 Hz, 1 H, 2-H, β anomer) ppm. ^{13}C NMR (125 MHz, $CDCl_3$): (β anomer): δ = 20.76 (CH_3, AcO), 20.88 (CH_3, AcO), 20.94 (CH_3, AcO), 20.99 (CH_3, AcO), 62.99 (CH_2, C-6), 65.98 (CH, C-4), 70.83 (CH, C-2), 72.15 (CH, C-3), 73.45 (CH, C-5), 82.37 (CH, C-1), 169.87 (CO, AcO), 170.21 (CO, AcO), 170.38 (CO, 2 AcO), 170.87 (CO, AcO). (α anomer): δ = 20.84 (CH_3, AcO), 20.92 (CH_3, AcO), 20.97 (CH_3, AcO), 21.10 (CH_3, AcO), 62.67 (CH_2, C-6), 66.91 (CH, C-4), 68.44 (CH, C-5), 69.16 (CH, C-3), 70.15 (CH, C-2), 81.15 (CH, C-1), 169.79 (CO, AcO), 170.14 (CO, AcO), 170.72 (CO, AcO), 170.98 (CO, AcO) ppm. MS (ES$^+$): m/z = 348 [M + H]$^+$, 370 [M + Na]$^+$, 695 [2M + H]$^+$. IR (film): $\tilde{\nu}$ = 3412, 2927, 1748, 1636, 1432, 1368, 1280, 1219, 1120, 1063, 1041, 961 cm^{-1}.

2,3,4-Tri-*O*-acetyl-6-deoxy-α/β-D-mannopyranose (12) and 1,2,3,4-Tetra-*O*-acetyl-6-deoxy-α/β-D-mannopyranose (13): A solution of compound **11** (2 g, 4.36 mmol) in MeOH (50 mL) was treated with Raney Nickel (7 g) and pyridine (0.1 mL), and the mixture was

hydrogenated for 4 d. The catalyst was removed by filtration, and the solvent was evaporated under reduced pressure. The residue was purified by column chromatography (SiO_2; hexane/EtOAc, 90:10) to give, in order of elution, **13**[22] (0.33 g, 23%), and **12** (0.75 g, 60%). Compound **12** is described as follows: R_f = 0.4 (hexane/EtOAc, 4:1). ^{1}H NMR ($CDCl_3$): for α isomer: δ = 1.2 (d, J = 6.3 Hz, 3 H, CH_3), 1.98 (s, 3 H, AcO), 2.05 (s, 3 H, AcO), 2.14 (s, 3 H, AcO), 3.18 (m, 1 H, 6-H, 6′-H), 4.12 (m, 1 H, 5-H), 5.06 (t, J = 9.9 Hz, 1 H, 4-H), 5.14 (s, 1 H, 1-H), 5.25 (dd, J = 1.8, 3.4 Hz, 1 H, 2-H), 5.36 (dd, J = 3.4, 10.1 Hz, 1 H, 3-H) ppm. ^{13}C NMR ($CDCl_3$): δ = 17.36 (CH_3), 20.65 (CH_3, AcO), 20.73 (CH_3, AcO), 20.85 (CH_3, AcO), 66.19 (C-5), 68.84 (C-3), 70.33 (C-2), 71.1 (C-4), 91.93 (C-1), 170.14 (CO, AcO), 170.2 (CO, AcO), 170.35 (CO, AcO) ppm. MS (ES^+): m/z (%) = 313.2 (100) $[M + Na]^+$, 273 (6) $[M - OH]^+$.

To convert **12** into a further amount of **13**, compound **12** (0.75 g, 2.586 mmol) was dissolved in pyridine (5 mL), and acetic anhydride (0.52 mL) was added. The reaction mixture was stirred overnight. The mixture was then concentrated, the residue was diluted with CH_2Cl_2, and the mixture was washed with HCl (1 M) and $NaHCO_3$. The organic layer was dried with Na_2SO_4, and filtered. The solvent was removed under reduced pressure to give compound **13** (0.81 g, 95%). This product was used without further purification.

2,3,4,6-Tetra-*O*-acetyl-6-deoxy-α/β-D-mannopyranosylamine (15): A solution of **14** (1 g, 3.17 mmol) and Pd/C (0.6 g) in dry CH_2Cl_2 (25 mL) was stirred under a hydrogen atmosphere overnight. The suspension was filtered, and the filtrate was evaporated to give amine **15** (0.87 g, 95%) as a mixture of α/β anomers (1:10), which was used without further purification in the next amide-bond formation. The β anomer is described as follows: R_f = 0.1 (hexane/EtOAc, 4:1). ^{1}H NMR (300 MHz, $CDCl_3$): δ = 1.21 (d, J = 6.17 Hz, 3 H, CH_3), 1.95 (s, 3 H, AcO), 2.02 (s, 3 H, AcO), 2.16 (s, 3 H, AcO), 3.51 (m, 1 H, 5-H), 4.4 (d, J = 1.16 Hz, 1 H, 1-H), 4.92–4.98 (m, 2 H, 3-H, 4-H), 5.36 (dd, J = 1.16, 2.98 Hz, 1 H, 2-H) ppm.

$(AcO)_4$-α/β-D-Man-Py-γ-Py-Ind (17): Compound **8** (0.228 g, 0.658 mol) and activated acid **16** (which was synthesized previously in our group)[10] (0.2 g, 0.33 mmol) were dissolved in anhydrous DMF (5 mL), and DIEA (85 μL, 0.658 mmol) was added. The reaction mixture was stirred at room temperature for 48 h. Compound **8** (0.2 g, 0.57 mmol) was added, and the reaction mixture was stirred for a further 92 h. When the reaction reached completion, the solvent was removed, and the residue was purified with column chromatography (toluene/MeOH, 10:1 to 8:1) to give compound **17** (189 mg, 70%) as a mixture of α/β anomers. The β anomer was characterized as follows: R_f = 0.3 (toluene/MeOH, 5:1). ^{1}H NMR (500 MHz, [D$_6$]DMSO): δ = 1.76–1.79 (m, 2 H, γ-b), 1.92 (s, 3 H, AcO), 2.00 (s, 3 H, AcO), 2.03 (s, 3 H, AcO), 2.17 (s, 3 H, AcO), 2.27 (t, J = 7.4 Hz, 2 H, γ-c), 3.20–3.22 (m, 2 H, γ-a), 3.77 (s, 3 H, MeA), 3.84 (s, 3 H, MeB), 3.99 (dd, J = 12.2, 2.3 Hz, 1 H, 6-H), 4.02–4.05 (m, 1 H, 5-H), 4.18 (dd, J = 12.2, 5.0 Hz, 1 H, 6′-H), 5.07 (d, J = 10.0 Hz, 1 H, 4-H), 5.24 (dd, J = 3.6, 1.3 Hz, 1 H, 2-H), 5.35 (dd, J = 10.2, 3.5 Hz, 1 H, 3-H), 5.81 (dd, J = 8.9, 1.4 Hz, 1 H, 1-H), 6.77 (d, J = 1.9 Hz, 1 H, Py-3B), 6.89 (d, J = 1.9 Hz, 1 H, Py-3A), 7.05 (ddd, J = 8.0, 6.9, 1.0 Hz, 1 H, Ind-5), 7.19 (ddd, J = 8.2, 7.0, 1.1 Hz, 1 H, Ind-6), 7.26–7.28 (m, 3 H, Ind-3, Py-5A, Py-5B), 7.46 (d, J = 8.2, 2.8 Hz, 1 H, Ind-7), 7.64 (dd, J = 8.0, 1.0 Hz, 1 H, Ind-4), 8.09 (t, J = 5.8 Hz, 1 H, 3-NH), 8.55 (d, J = 8.8 Hz, 1 H, 5-NH), 9.82 (s, 1 H, 4-NH), 10.28 (s, 1 H, 2-NH), 11.59 (d, J = 2.2 Hz, 1-NH) ppm. ^{13}C NMR (125 MHz, [D$_6$]-DMSO): δ = 20.4 (CH_3, AcO), 20.5 (CH_3, AcO), 20.6 (CH_3, AcO), 21.0 (CH_3, AcO), 25.7 (CH_2, γ-b), 33.2 (CH_2, γ-c), 36.1 (CH_3, MeA), 36.2 (CH_3, MeB), 38.2 (CH_2, γ-a), 62.3 (CH, C-6), 65.4 (CH, C-4), 68.4 (CH, C-2), 70.9 (CH, C-3), 72.9 (CH, C-5), 77.2 (CH, C-1), 102.8 (CH, Ind-3), 104.1 (CH, Py-3A), 105.4 (CH, Py-3B), 112.3 (CH, Ind-7), 118.1 (CH, Py-5A), 119.2 (CH, Py-5B), 119.8 (CH, Ind-5), 121.3 (C, PyB), 121.5 (CH, Ind-4), 121.6 (C, PyA), 121.9 (C, PyB), 123.2 (C, PyA), 123.4 (CH, Ind-6), 127.1 (C, Ind-3a), 131.7 (C, Ind-2), 136.6 (C, Ind-7a), 158.2 (CO), 160.4 (CO), 161.2 (CO), 169.3 (CO), 169.5 (CO, AcO), 169.6 (CO, AcO), 170.0 (CO, AcO), 170.4 (CO, AcO) ppm. MS (ES^+): m/z = 1641 $[2M + H]^+$ 843 $[M + Na]^+$, 820 $[M + H]^+$. IR (KBr): $\tilde{\nu}$ = 3428, 2934, 1644, 1517, 1438, 1368 cm^{-1}. $C_{39}H_{45}N_7O_{13}$ (819.3075): calcd. C 55.67, H 5.49, N 11.95; found C 55.80, H 5.83, N 11.64.

$(AcO)_4$-α/β-L-Man-Py-γ-Py-Ind (18): Compound **9** (280 mg, 0.82 mmol) and compound **16** (250 mg, 0.41 mmol) were dissolved in anhydrous DMF (4 mL), and DIEA (258 ul, 1.6 mmol) was added. The mixture was stirred at room temperature. After 92 h, toluene was added to the reaction mixture, and then the solvent was evaporated under reduced pressure. The residue was purified by column chromatography (SiO_2, EtOAc) to give compound **18** (94 mg, 28%) as a mixture of anomers α/β (1:4). An analytical sample of the β anomer was characterized as follows: R_f = 0.45 (EtOAc/MeOH, 20:1), m.p. 138–140 °C. ^{1}H NMR (500 MHz, [D$_6$]DMSO): δ = 1.76–1.79 (m, 2 H, γ-b), 1.92 (s, 3 H, AcO), 2.00 (s, 3 H, AcO), 2.03 (s, 3 H, AcO), 2.17 (s, 3 H, AcO), 2.27 (t, J = 7.4 Hz, 2 H, γ-c), 3.20–3.22 (m, 2 H, γ-a), 3.77 (s, 3 H, MeA), 3.84 (s, 3 H, MeB), 3.99 (dd, J = 12.2, 2.3 Hz, 1 H, 6-H), 4.02–4.05 (m, 1 H, 5-H), 4.18 (dd, J = 12.2, 5.0 Hz, 1 H, 6′-H), 5.07 (d, J = 10.0 Hz, 1 H, 4-H), 5.24 (dd, J = 3.6, 1.3 Hz, 1 H, 2-H), 5.35 (dd, J = 10.2, 3.5 Hz, 1 H, 3-H), 5.81 (dd, J = 8.9, 1.4 Hz, 1 H, 1-H), 6.77 (d, J = 1.9 Hz, 1 H, Py-3B), 6.89 (d, J = 1.9 Hz, 1 H, Py-3A), 7.05 (ddd, J = 8.0, 6.9, 1.0 Hz, 1 H, Ind-5), 7.19 (ddd, J = 8.2, 7.0, 1.1 Hz, 1 H, Ind-6), 7.26–7.28 (m, 3 H, Ind-3, Py-5A, Py-5B), 7.46 (d, J = 8.2, 2.8 Hz, 1 H, Ind-7), 7.64 (dd, J = 8.0, 1.0 Hz, 1 H, Ind-4), 8.09 (t, J = 5.8 Hz, 1 H, 3-NH), 8.55 (d, J = 8.8 Hz, 1 H, 5-NH), 9.82 (s, 1 H, 4-NH), 10.28 (s, 1 H, 2-NH), 11.59 (d, J = 2.2 Hz, 1-NH) ppm. ^{13}C NMR (125 MHz, [D$_6$]DMSO): δ = 20.4 (CH_3, AcO), 20.5 (CH_3, AcO), 20.6 (CH_3, AcO), 21.0 (CH_3, AcO), 25.7 (CH_2, γ-b), 33.2 (CH_2, γ-c), 36.1 (CH_3, MeA), 36.2 (CH_3, MeB), 38.2 (CH_2, γ-a), 62.3 (CH, C-6), 65.4 (CH, C-4), 68.4 (CH, C-2), 70.9 (CH, C-3), 72.9 (CH, C-5), 77.2 (CH, C-1), 102.8 (CH, Ind-3), 104.1 (CH, Py-3A), 105.4 (CH, Py-3B), 112.3 (CH, Ind-7), 118.1 (CH, Py-5A), 119.2 (CH, Py-5B), 119.8 (CH, Ind-5), 121.3 (C, PyB), 121.5 (CH, Ind-4), 121.6 (C, PyA), 121.9 (C, PyB), 123.2 (C, PyA), 123.4 (CH, Ind-6), 127.1 (C, Ind-3a), 131.7 (C, Ind-2), 136.6 (C, Ind-7a), 158.2 (CO-1), 160.4 (CO-4), 161.2 (CO-2), 169.3 (CO-3), 169.5 (CO, AcO), 169.6 (CO, AcO), 170.0 (CO, AcO), 170.4 (CO, AcO) ppm. HRMS (ESI^+): calcd. for $C_{39}H_{46}N_7O_{13}$ $[M + H]^+$ 820.3148; found 820.3181. IR (KBr): $\tilde{\nu}$ = 3421, 2135, 1749, 1649, 1592, 1526, 1438, 1403, 1369, 1306, 1242, 1146, 1054, 813, 748, 672, 599 cm^{-1}. $C_{39}H_{45}N_7O_{13}$ (819.81) calcd. C 57.14, H 5.53, N 11.96; found C 57.02, H 5.63, N 12.13.

$(AcO)_3$-6-deoxy-α/β-D-Man-Py-γ-Py-Ind (19): This compound was prepared from **16** (0.3 g, 0.49 mmol) and **15** (0.23 g, 0.79 mmol) as described above for the synthesis of compound **18**. The residue was purified by column chromatography (SiO_2; toluene/MeOH, 10:1 to 8:1) to give compound **19** (189 mg, 70%) as a mixture of α/β anomers. The β anomer was characterized as follows: R_f = 0.3 (toluene/MeOH, 5:1). ^{1}H NMR (300 MHz, [D$_6$]DMSO): δ = 11.6 (s, 1 H, NH), 10.29 (s, 1 H, NH), 9.83 (s, 1 H, NH), 8.46 (d, J = 8.76 Hz, NH), 8.10 (t, J = 4.5 Hz, NH), 7.63 (d, J = 7.95 Hz, 4-H-Ind), 7.44 (d, J = 8.4 Hz, 7-H-Ind), 7.26 (m, 3 H, 3-H-Ind and H-Py), 7.18 (t, J = 7.2 Hz, 6-H-Ind), 7.03 (t, J = 8.1 Hz, 5-H-Ind), 6.88 (d, J = 1.8 Hz, 3-H-Py), 6.70 (d, J = 1.8 Hz, 3-H-Py), 5.71 (d, J = 8.4 Hz,

1-H), 5.02–5.28 (m, 2 H), 4.85 (m, 1 H), 3.79 (m, 5-H), 3.83 (s, 3 H, CH_3), 3.74 (s, 3 H, CH_3), 3.22 (m, 2 H,CH_2-γ), 2.26 (m, 2 H, CH_2-γ), 2.16 (s, 3 H, CH_3), 2.05 (s, 3 H, CH_3), 1.91 (s, 3 H, CH_3), 1.77 (m, 2 H,CH_2-γ), 1.12 (d, J = 6.3 Hz, CH_3) ppm. ^{13}C NMR (75 MHz, [D$_6$]DMSO): δ = 171 (CO), 170.5 (CO), 170.1 (CO), 170 (CO), 162.4 (CONH), 160.6 (CONH), 159.2 (CONH), 136.6 (CONH), 130.9 (C), 127.7 (C), 124.7 (C), 123.4 (C), 122.1 (C), 121.8 (C), 121.7 (C), 120.9 (C), 120.8 (C), 120.35 (C), 119.4 (C), 112.0 (C), 104.7 (C), 104.4 (C), 103.06 (C), 103.0 (C), 76.2 (CH), 73.34 (CH), 71.7 (CH), 70.7 (CH), 70.3 (CH), 38.6 (CH_2), 36.6 (CH_2), 34.04 (CH_2), 33.41 (CH_2), 25.77 (CH_2), 20.9 (CH_3CO), 20.8 (CH_3CO), 20.62 (CH_3CO), 17.5 (CH_3) ppm. MS (ES$^+$): m/z (%) = 685 (10) [M + Na]$^+$, 762 (100) [M + H]$^+$. IR (KBr): ṽ = 3422, 2934, 1750, 1646, 1514, 1438, 1402, 1370 cm^{-1}.

β-D-Man-Py-γ-Py-Ind (1): A solution of **17** (171 mg, 0.21 mmol) in MeOH (6 mL) was treated with a solution of NaOMe (45 mg, 0.83 mmol) in MeOH (1 mL). This resulted in an immediate deeper yellow colour that indicated that the reaction was complete. The solution was acidified to pH 6 with Amberlite IR-120 ion-exchange resin. The resin was removed by filtration, and the solvent was evaporated. The residue was purified by column chromatography (CH_2Cl_2/MeOH/toluene, 5:2:1) to give **1** (108 mg, 79%). R_f = 0.12 (CH_2Cl_2/MeOH/H_2O, 6:1:0.1), m.p. 187–190 °C. [a]$_D$ = + 9.61 (c = 0.77, MeOH). ^{1}H NMR (500 MHz, [D$_6$]DMSO): δ = 1.76–1.82 (m, 2 H, γ-b), 2.27 (t, J = 7.5 Hz, 2 H, γ-c), 3.10 (ddd, J = 9.3, 6.0, 2.2 Hz, m, 1 H, 5-H), 3.22 (q, J = 6.6 Hz, 2 H, γ-a), 3.33–3.45 (m, 3 H, 3-H, 4-H, 6-H), 3.63–3.66 (m, 1 H, 2-H), 3.65–3.68 (m, 1 H, 6′-H), 3.79 (s, 3 H, MeA), 3.84 (s, 3 H, MeB), 4.46 (t, J = 5.9 Hz, 1 H, 6-OH), 4.73 (t, J = 5.48 Hz, 2 H, 3-OH, 4-OH), 5.10 (d, J = 4.4 Hz, 1 H, 2-OH), 5.13 (d, J = 9.3 Hz, 1-H), 6.69 (d, J = 1.9 Hz, 1 H, Py-3B), 6.89 (d, J = 1.9 Hz, Py-3A), 7.05 (ddd, J = 8.0, 6.9, 1.0 Hz, 1 H, Ind-5), 7.17–7.21 (m, 2 H, Ind-6, P-5B), 7.28 (m, 2 H, Ind-3, Py-5A), 7.46 (d, J = 9.2 Hz, 1 H, Ind-7), 7.49 (d, J = 9.2 Hz, 1 H, 5-NH), 7.64 (dd, J = 8.0, 0.9 Hz, 1 H, Ind-4), 8.11 (t, J = 5.7 Hz, 1 H, 3-NH), 9.83 (s, 1 H, 4-NH), 10.29 (s, 1 H, 2-NH), 11.61 (d, J = 2.2 Hz, 1-NH) ppm. ^{13}C NMR (125 MHz, [D$_6$]-DMSO): δ = 25.6 (CH_2, γ-b), 33.3 (CH_2, γ-c), 36.0 (CH_3, MeA), 36.1 (CH_3, MeB), 38.22 (CH_2, γ-a), 61.2 (CH, C-6), 66.6 (CH, C-4), 70.6 (CH, C-2), 73.9 (CH, C-3), 77.1 (CH, C-1), 78.9 (CH, C-5), 102.8 (CH, Ind-3), 103.7 (CH, Py-3B), 104.0 (CH, Py-3A), 112.2 (CH, Ind-7), 118.1 (CH, Py-5A), 118.7 (CH, Py-5B), 119.8 (CH, Ind-5), 121.5 (CH, Ind-4), 121.5 (C, Py-4B), 121.6 (C, Py-2B), 122.2 (C, Py-4A), 123.1 (C, Py-2A), 123.3 (CH, Ind-6), 127.0 (C, Ind-3a), 131.6 (C, Ind-2), 136.5 (C, Ind-7a), 158.2 (CO), 159.9 (CO), 161.2 (CO), 169.3 (CO) ppm. HRMS (ESI$^+$): calcd. for $C_{31}H_{38}N_7O_9$ [M + H]$^+$ 652.2726; found 652.2726. IR (KBr): ṽ = 3412, 2930, 2935, 1642, 1589, 1519 cm^{-1}. $C_{31}H_{37}N_7O_9$ (651.67): calcd. C 57.14, H 5.72, N 15.05; found C 57.19, H 5.90, N 15.49.

β-L-Man-Py-γ-Py-Ind (2): Compound **2** was prepared from **18** (40 mg, 0.05 mmol) as described above for the synthesis of compound **1**. The residue was purified by column chromatography (CH_2Cl_2/MeOH/H_2O, 6:1:0.1) to give compound **2** (22 mg, 70%). R_f = 0.12 (CH_2Cl_2/MeOH/H_2O, 6:1:0.1), m.p. 150–155 °C. [a]$_D$ = –10.7 (c = 0.8, MeOH). ^{1}H NMR (500 MHz, [D$_6$]DMSO): δ = 1.76–1.82 (m, 2 H, γ-b), 2.27 (t, J = 7.5 Hz, 2 H, γ-c), 3.10 (ddd, J = 9.3, 6.0, 2.2 Hz, m, 1 H, 5-H), 3.22 (q, J = 6.6 Hz, 2 H, γ-a), 3.33–3.45 (m, 3 H, 3-H, 4-H, 6-H), 3.63–3.66 (m, 1 H, 2-H), 3.65–3.68 (m, 1 H, 6′-H), 3.79 (s, 3 H, MeA), 3.84 (s, 3 H, MeB), 4.46 (t, J = 5.9 Hz, 1 H, 6-OH), 4.73 (t, J = 5.48 Hz, 2 H, 3-OH, 4-OH), 5.10 (d, J = 4.4 Hz, 1 H, 2-OH), 5.13 (d, J = 9.3 Hz, 1-H), 6.69 (d, J = 1.9 Hz, 1 H, Py-3B), 6.89 (d, J = 1.9 Hz, Py-3A), 7.05 (ddd, J = 8.0, 6.9, 1.0 Hz, 1 H, Ind-5), 7.17–7.21 (m, 2 H, Ind-6, P-5B), 7.28 (m, 2 H, Ind-3, Py-5A), 7.46 (d, J = 9.2 Hz, 1 H, Ind-7), 7.49 (d, J = 9.2 Hz, 1 H, 5-NH), 7.64 (dd, J = 8.0, 0.9 Hz, 1 H, Ind-4), 8.11 (t, J = 5.7 Hz, 1 H, 3-NH), 9.83 (s, 1 H, 4-NH), 10.29 (s, 1 H, 2-NH), 11.61 (d, J = 2.2 Hz, 1-NH) ppm. ^{13}C NMR (125 MHz, [D$_6$]DMSO): δ = 25.6 (CH_2, γ-b), 33.27 (CH_2, γ-c), 36.06 (CH_3, MeA), 36.12 (CH_3, MeB), 38.18 (CH_2, γ-a), 70.82 (CH, C-2), 71.73 (CH, C-4), 73.48 (CH, C-5), 73.72 (CH, C-3), 77.15 (CH, C-1), 102.80 (CH, Ind-3), 103.89 (CH, Py-3B), 104.08 (CH, Py-3A), 112.29 (CH, Ind-7), 118.09 (CH, Py-5A), 118.76 (CH, Py-5B), 119.77 (CH, Ind-5), 121.52 (CH, Py-4A), 121.62 (CH, Ind-4), 121.71 (CH, Py-2B), 122.24 (CH, Py-4B), 123.22 (CH, Py-2A), 123.36 (CH, Ind-6), 127.12 (C, Ind-3a), 131.65 (C, Ind-2), 136.57 (C, Ind-7a), 158.19 (CO), 160.03 (CO), 161.19 (CO), 169.25 (CO) ppm. HRMS (ESI$^+$) calcd. for $C_{31}H_{37}N_7O_8$ [M + H]$^+$ 636.2776; found 636.2771. IR (KBr): ṽ = 3429, 2930, 1640, 1591, 1518, 1645, 1438, 1403, 1341, 1307, 1250, 1146, 1067, 1014, 892, 748, 576 cm^{-1}. $C_{31}H_{37}N_7O_8$ (635.68): calcd. C 58.57, H 5.87, N 15.42; found C 58.49, H 5.79, N 15.62.

Sample Preparation for NMR Experiments: Calf thymus DNA (ct-DNA) and poly(dA-dT)$_2$ were purchased from Sigma–Aldrich, and were used without further purification.

^{1}H NMR Spectroscopy: All spectra in aqueous solution were recorded with presaturation of the water signal. Chemical shifts are reported in ppm relative to [D$_4$](trimethylsilyl)propionic acid (δ = 0.00 ppm) when D_2O at 25 °C and H_2O at 5 °C was used in the experiment. NMR structural studies of compounds **1**–**3** in the free state were based on one-dimensional and two-dimensional (TOCSY, HSQC, NOESY, ROESY) experiments recorded at 500 MHz with a Bruker Avance spectrometer. Sample solutions were prepared at concentrations in the range 10^{-4}–10^{-3} M depending on the solubility of the compounds.

Bound-State NMR Spectroscopic Experiments (TR-NOESY and Differential Frequency STD Experiments): These experiments were

carried out in phosphate buffer (10 mM, pH 7). Ligand samples were prepared at a concentration of 10^{-4} M. The ct-DNA and poly-(dA-dT)$_2$ (stock solution) was prepared by dissolving the DNA polymers (2 mg) in D_2O (700 μL). The concentration of ct-DNA was calculated by UV/Vis spectroscopy ($c \approx 10^{-3}$ M, ε = 13200 $M^{-1}cm^{-1}$ for ct-DNA and ε = 12824 $M^{-1}cm^{-1}$).[23] The NMR spectroscopic sample was prepared by titration of the ligand solution (0.5 mL) with increasing amounts of the titrant DNA solution to reach a DNA/ligand ratio of 4:1 in all cases. The bound-state NMR experiments were carried out once the spectra of the free ligand was clear but slightly broadened. The same NMR tube was used for both the TR-NOESY and STD experiments in every case.

TR-NOESY Experiments: TR-NOESY experiments for the bound ligand were performed with a Bruker Avance 500 spectrometer with saturation of the residual H_2O signal or with the Watergate pulse sequence. TR-NOESY experiments were recorded at 25 °C with mixing times of 200 ms.

STD Experiments: STD experiments for the bound ligands were performed with a 500 MHz Bruker Avance spectrometer using D_2O as solvent. Either no water suppression or the Watergate sequence was used, depending on the signal/noise ratio obtained without solvent suppression. A ligand/receptor molar excess of up to 4:1 for all ligands was used for the best STD effects. The STD effects of the individual protons were calculated for each compound relative to a reference spectrum with off-resonance saturation at δ = 100 ppm. For the reference STD spectrum, 128 scans were recorded. The best duration of the saturation pulse, the power of the selective Gaussian pulse, and the recycling delay were optimized to get the best possible signal/noise ratio with no spin diffusion within a reasonable experimental time. The final experiments were performed at 298 K with a recycling delay of 4 s, an acquisition time of around 1.3 s, and a saturation time of 400 ms. The saturation was accomplished by using 8 Gaussian-shaped pulses of 49 ms each, separated by 1 ms, with an approximate power of γB = 20 Hz. Two saturation frequencies were selected: δ = 4.5 ppm (to reach the 4′-H, 5′-H, and 5′′-H region of deoxyribose in DNA), and δ = 5.6 ppm (to reach the 1′-H region in DNA). Control experiments performed without the DNA receptor showed that no effect could be observed in the ligand protons when the 1′-H region (δ = 5.60 ppm) in DNA was chosen, whereas >5% saturation was observed for some ligands at the anomeric 1-H, MeA, and MeB for on-resonance saturation at δ = 4.50 ppm. The intensities due to saturation observed in the control experiments were subtracted from the intensities observed in the presence of DNA to calculate the STD intensities. The intensity of each peak in the STD spectra was standardized relative to a proton-resonance intensity that was designated to be 100. The normalization of the signal intensity was done relative to Py3A. Such conclusions were obtained by comparing the normalized value of each proton-resonance intensity upon irradiation of the outer or inner region of the groove.

Dissociation Constant Calculations: Ligand samples were prepared at a concentration of 10^{-4} M. The poly(dA-dT)$_2$ titrant sample (stock solution) was prepared by dissolving the DNA (2 mg) in a 10^{-4} M solution of ligand (700 μL). The NMR spectroscopic sample was prepared by titration of the ligand solution (0.5 mL) with increasing amounts of poly(dA-dT)$_2$ solution with the ligand concentration kept constant. A 1D spectrum was recorded in the same "acquisition mode" (No. of scans = 64, T = 25 °C) after each addition of poly(dA-dT)$_2$. A progressive broadening and disappearance of the proton signals from the ligand was observed; this indicates binding of the ligand to poly(dA-dT)$_2$.

A set of 1D ^{1}H NMR spectra were acquired for each DNA ligand at different concentrations of polynucleotide, and the intensities of the ligand NMR signals were monitored. The concentration of the ligand was kept constant, while the concentration of the macromolecule was systematically increased in the different additions.

The ^{1}H NMR peak-intensity ratios (I_{obs}/I_0) in the presence (I_{obs}) and absence (I_0) of the macromolecule are related to the fraction of the bound ligand. Thus, when the ligand binds to the DNA, its relaxation properties change drastically. A dramatic line-broadening is observed, with a concomitant decrease in the signal intensities.[24] In particular, we monitored the signal intensities of the aromatic resonances of the ligand upon increasing the amount of the macromolecule. As example, Figure S31A in the Supporting Information shows the decrease in the intensities of the ^{1}H NMR signals of **1** upon addition of increasing amounts of poly(dA-dT)$_2$. Changes in the signal intensity of the [D$_4$]trimethylsilylpropionic acid reference were not observed (Figure S30B in the Supporting Information), indicating that the variations in the peaks of **1** are due to a binding event.

The dissociation constants K_d were estimated using Equation (1) for data fitting, based on the procedure described by Shortridge et al.[24]

$$\frac{I_{obs}}{I_0} = \frac{1}{1 + cf_B} \quad (1)$$

In Equation (1), f_B is the fraction of the ligand bound to DNA, and can be expressed in terms of K_d and [poly(dA-dT)$_2$] (See Supporting Information). The nondimensional parameter (c) is defined as $c = (\nu_B/\nu_F - 1)$, where ν_B and ν_F correspond to the line-width of the resonances of the ligand in the free and the bound states, respectively. The ratio represents the proportional change in the line-width of the ligand when it is bound to DNA, and acts as a scaling factor for the calculation of the K_d value. Unfortunately, the reduction in signal intensity to below observable levels before binding saturation could be achieved impedes a precise estimate of the c value; this can result in a systematic underestimation or overestimation of K_d. However, although the calculated values of K_d will be inaccurate, the ranking of the ligand binding affinities would be maintained. We assume that all of the compounds bind in a very close geometry, so the broadening for a particular proton will be the same, independent of the compound, when the ligand reaches the same bound molar fraction. A limiting lower value of c for each type of proton was estimated from the highest value observed among all compounds.

Equation (1) can be rearranged into the following form (see Supporting Information).

Equation (2) assumes an interaction model for a complex with 1:1 stoichiometry.

$$\frac{I_{obs}}{I_0} = \frac{1}{1 + \frac{c \cdot [P]_T}{[P]_T + K_D}} \quad (2)$$

The K_d values were obtained from nonlinear-regression fitting of the experimental data using Equation (2). In the data fitting, the c parameter was kept constant for each proton type, and K_d was treated as adjustable parameter.

Competition Experiments: For these experiments, a ^{1}H NMR spectrum of the buffer solution containing both ligands **1** and **3** in the same concentration (155 μM) was recorded. Then further ^{1}H NMR

spectra were recorded after adding increasing amounts of poly-(dA-dT)$_2$ (5–6 mM base pair). The intensities of the resonances of the ligand with the higher affinity for the DNA diminish more quickly.

For the competition of **1** vs. **3** with poly(dA-dT)$_2$, the aromatic region of the spectra of the two ligands did not show any resonance overlap (Figure 7), so a solution of equal concentrations of **1** and **3** was prepared in D_2O (in 6.1 mM Na_2HPO_4, 3.9 mM NaH_2PO_4 buffer, pH = 7.2), and the corresponding ^1H NMR spectrum was recorded. Then, increasing amounts of poly(dA-dT)$_2$ were added (Figure 7). Examination of the aromatic region of the spectra of the ligands upon addition of the macromolecule showed that the resonances of **1** significantly broadened, and their intensity was diminished at an earlier addition point compared to those of **3**. Figure S35 in the Supporting Information shows the decay of the intensity ratios as a function of the amount of DNA added.

MD Simulations: The interaction between **2** (β-L-Man) with a double-strand dodecamer d(AT)$_{12}$ model was studied using MD simulations. The geometry of the complex was built up by docking the free-state structure obtained for the mannose ligand in the polyAT DNA model constructed with the xLeaP Amber module.

An MD simulation with no restraints in an explicit solvent was performed using the SANDER module in Amber 9.0.[25]

The ligand needed to be prepared for its use in the Amber package. The RESP atomic charges were derived for the ligand in a systematic way, which involved fragmentation of the system into two pieces, with the vector on one side (which was described by the general Gaff Amber force field)[26] and the sugar moiety (which followed the Glycam 06 force field)[27] on the other side. The RED server protocol, which automated the procedure, was used for this purpose.[28] The two moieties were brought together in the XLEaP module from Amber to prepare the input files for the simulation. Both the DNA models were described with force-field 99 (ff99).[29]

MD simulations in an explicit solvent were carried out using a truncated octahedral box with dimensions of 10.0 Å for the explicit TIP3P water molecules.[30] A total of 24 sodium ions were added as counterions to neutralize the DNA charges. The simulation was performed using periodic boundary conditions, and the particle-mesh Ewald approach[31] to account for the electrostatic interactions. The protocol included four steps. An initial minimization restrained on the corresponding DNA molecule and the *glyco*-oligoamide, to place the water molecules properly, followed by a minimization of the whole system. A simulation of position-restrained dynamics for 20 ps was carried out to relax the locations of the solvent molecules and to heat the system. Finally, 1 ns of an unrestrained MD simulation at 300 K and 1 atm was recorded, with 5596 structures saved for further analysis.

The final frames were processed and clusterized using the Amber module, and the most representative structure was selected for discussion.

Acknowledgments

This work was supported by the Spanish Ministry of Economy and Competitiviness (MEC) (projects CTQ-10847-C02-01, CTQ-10847-C02-02, CTQ2009-10547, and CTQ2012-32025), and the European Cooperation in Science and Technology, COST Action CM1102. M. C. F. A. thanks the Consejo Superior de Investigaciones Científicas (JAE-Doc CSIC program) for financial support. F. M. thanks the Portuguese Fundo Europeu de Desenvolvimento Regional (FCT) for a post-doctoral research grant (SFRH/BPD/65462/2009). R. V. G. thanks the Ministerio of Education for FPU predoctoral fellowships.

[1] a) B. Meyer, T. Peters, *Angew. Chem. Int. Ed.* **2003**, *42*, 864–890; *Angew. Chem.* **2003**, *115*, 890–918; b) V. Roldós, F. Cañada, J. Jiménez-Barbero, *ChemBioChem* **2011**, *12*, 990–1005.
[2] a) F. A. Quiocho, *Philos. T. R. Soc. B* **1990**, *326*, 341–351; b) F. A. Quiocho, *Annu. Rev. Biochem.* **1986**, *55*, 287–315.
[3] P. Peñalver, F. Marcelo, J. Jiménez-Barbero, C. Vicent, *Chem. Eur. J.* **2011**, *17*, 4561–4570.
[4] H. S. Frank, W. Wen-Yan, *Discuss. Faraday Soc.* **1957**, *24*, 133–140.
[5] a) V. Vicente, J. Martin, J. Jiménez-Barbero, J. L. Chiara, C. Vicent, *Chem. Eur. J.* **2004**, *10*, 4240–4251; b) E. M. Muñoz, M. López de la Paz, J. Jiménez-Barbero, G. Ellis, E. M. Pérez, C. Vicent, *Chem. Eur. J.* **2002**, *8*, 1908–1914; c) J. Hawley, N. Bampos, N. Aboitiz, J. Jiménez-Barbero, M. Lopez de la Paz, J. Sanders, K. M. P. Carmona, C. Vicent, *Eur. J. Org. Chem.* **2002**, 1925–1936; d) M. Lopez de la Paz, C. González, C. Vicent, *Chem. Commun.* **2000**, 411–412; e) M. López de la Paz, G. Ellis, S. Penadés, C. Vicent, *Tetrahedron Lett.* **1997**, *38*, 1659–1662.
[6] J. L. Asensio, F. Cañada, H. C. Siebert, J. Laynez, A. Poveda, P. Nieto, U. M. Soedjanaamadja, H. J. Gabius, J. Jiménez-Barbero, *Chem. Biol.* **2000**, *7*, 529–543.
[7] M. T. Blázquez-Sánchez, F. Marcelo, M. C. Fernández-Alonso, A. Poveda, J. Jiménez-Barbero, C. Vicent, *Chem. Eur. J.* **2014**, *20*, 17640–17652.
[8] X. Qu, J. O. Trent, I. Fokt, W. Priebe, J. B. Chaires, *Proc. Natl. Acad. Sci. USA* **2000**, *97*, 12032–12037.
[9] D. M. Herman, E. E. Baird, P. B. Dervan, *J. Am. Chem. Soc.* **1998**, *120*, 1382–1391.
[10] C. Badía, F. Souard, C. Vicent, *J. Org. Chem.* **2012**, *77*, 10870–10881.
[11] H. Paulsen, Z. Györgydeák, M. Friedmann, *Chem. Berichte.* **1974**, *107*, 1568–1578.
[12] C. Rao, *J. Chem. Soc. Perkin Trans. 1* **1993**, 1207–1211.
[13] a) H. Paulsen, *Liebigs Ann.* **1995**, 67–76; b) D. Lafont, P. Boullanger, O. Cadas, G. Descotes, *Synthesis* **1989**, 191–194.
[14] F. Hong, E. Fan, *Tetrahedron Lett.* **2001**, *42*, 6073–6076.
[15] J. N. Martin, E. M. Munoz, C. Schwergold, F. Souard, J. L. Asensio, J. Jimenez-Barbero, J. Canada, C. Vicent, *J. Am. Chem. Soc.* **2005**, *127*, 9518–9533.
[16] S. Di Micco, C. Bassarello, G. Bifulco, R. Riccio, L. Gomez-Paloma, *Angew. Chem.* **2006**, *118*, 230–234.
[17] F. Souard, E. Muñoz, P. Peñalver, C. Badía, R. del Villar-Guerra, J. L. Asensio, J. Jiménez-Barbero, C. Vicent, *Chem. Eur. J.* **2008**, *14*, 2435–2442.
[18] E. Lee, A. Bruzzi, E. O'Brien, P. O'Colla, *Carbohydr. Res.* **1979**, *71*, 331–334.
[19] M. Ponpipom, R. Bugianesi, T. Y. Shen, *Carbohydr. Res.* **1980**, *82*, 141–148.
[20] F. Konishi, S. Esaki, S. Kamiya, *Agric. Biol. Chem.* **1983**, *47*, 1629–1631.
[21] P. J. Garegg, B. Samuelsson, *J. Chem. Soc. Perkin Trans. 1* **1980**, 2866–2869.
[22] W. Korytnyk, *J. Chem. Soc.* **1959**, 650–656.
[23] a) R. D. Wells, R. C. Grant, B. E. Shortle, C. R. Cantor, *J. Mol. Biol.* **1970**, *54*, 465–497; b) M. S. Gopal, S. R. Inamdar, *Proc. Indian Acad. Sci. Chem. Sci.* **2002**, *114*, 687–696; c) P. Ragazzon, J. Garbett, J. B. Chaires, *Methods* **2007**, *42*, 173–182.
[24] M. Shortridge, D. S. Shortridge, G. Hage, M. Harbison, M. Powers, *J. Comb. Chem.* **2008**, *10*, 948–958.
[25] D. A. Case, T. A. Darden, T. E. Cheatham III, C. L. Simmerling, J. Wang, R. E. Duke, R. Luo, K. M. Merz, D. A. Pearlman, M. Crowley, R. C. Walker, W. Zhang, B. Wang, S. Hayik, A. Roitberg, G. Seabra, K. F. Wong, F. Paesa, X. Wu, S. Brozell, V. Tsui, H. Gohlke, L. Yang, C. Tan, J. Mongan, V. Hornak, G. Cui, P. Beroza, D. H. Mathews, C. Schafmeister,

W. S. Ross, P. A. Kollman, *AMBER 9*, University of California, San Francisco, **2006**.
[26] J. Wang, W. Wolf, J. W. Caldwell, P. A. Kollman, D. A. Case, *J. Comput. Chem.* **2004**, *25*, 1157–1174.
[27] K. N. Kirschner, A. B. Yongye, S. M. Tschampel, J. González-Outeirino, C. R. Daniels, B. L. Foley, R. J. Woods, *J. Comput. Chem.* **2008**, *29*, 622–655.
[28] S. S. E. Vanquelef, G. Marquant, E. Garcia, C. Klimerak, J. C. Delepine, P. Cieplak, F. Y. Dupradeau, *Nucleic Acids Res.* **2011**, *39*, W511–W517 (web server issue).
[29] J. Wang, P. Cieplak, P. Kollman, *J. Comput. Chem.* **2000**, *21*, 1049–1074.
[30] W. Jorgensen, J. Chandrasekhar, J. Madura, R. Impey, M. Klein, *J. Chem. Phys.* **1983**, *79*, 926.
[31] M. W. Mahoney, J. Jorgensen, *J. Chem. Phys.* **2000**, *112*, 8910–8922.

Received: June 3, 2015
Published Online: August 17, 2015

